CHEMISTRY OF MATERIALS
Cite This: Chem. Mater. 2018, 30, 7456−7463
Article
pubs.acs.org/cm

Aluminum Oxide Thin Films from Aqueous Solutions: Insights from Solid-State NMR and Dielectric Response

Jinlei Cui,[†,#] Matthew G. Kast,[‡,#] Blake A. Hammann,[†] Yvonne Afriyie,[†] Keenan N. Woods,[‡] Paul N. Plassmeyer,[‡] Cory K. Perkins,[§] Zayd L. Ma,[†] Douglas A. Keszler,[§] Catherine J. Page,*[,‡] Shannon W. Boettcher,*[,‡] and Sophia E. Hayes*[,†]

[†]Department of Chemistry and Institute for Materials Science & Engineering, Washington University, St. Louis, Missouri 63130, United States

[‡]Department of Chemistry and Biochemistry, University of Oregon, Eugene, Oregon 97403, United States

[§]Department of Chemistry, Oregon State University, Corvallis, Oregon 97331, United States

Supporting Information

ABSTRACT: Here, we employ a combination of ^{27}Al solid-state nuclear magnetic resonance (SSNMR) and conventional spectroscopic and microscopic techniques to investigate the structural evolution of aqueous aluminum precursors to a uniform and smooth aluminum oxide film. The route involves no organic ligands and relies on dehydration, dehydroxylation, and nitrate loss for condensation and formation of the three-dimensional aluminum oxide structure. Local chemical environments are tracked as films evolve over the temperature range 200−1100 °C. ^{27}Al SSNMR reveals that Al centers are predominantly four- and five-coordinate in amorphous films annealed between 200 and 800 °C and four- and six-coordinate in crystalline phases that form above 800 °C. The Al coordination of the aqueous-deposited aluminum oxide films are compared to data from SSNMR studies on vapor-phase-deposited aluminum oxide thin films. Additionally, dielectric constants of aluminum oxide-based capacitors are measured and correlated with the SSNMR results. Aluminum oxide is an important material for protective coatings, catalysis, and microelectronic applications. For the latter application, amorphous materials are preferred, but a lack of long-range order complicates structural characterization and determination of structure−property relationships. Solution deposition approaches are attractive alternatives to traditional vapor-phase deposition methods because precursors are commonly stable in air, and they enable printing and direct lithographic patterning on common semiconductor wafers as well as large-area and flexible substrates—useful for scale-up to applications in windows and photovoltaic devices.

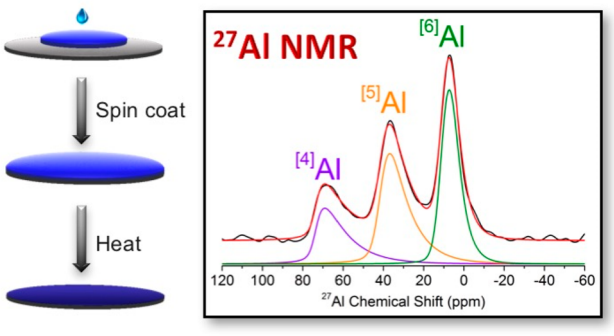

INTRODUCTION

Aluminum oxide (Al_2O_3) displays a number of important properties that make it a critical component in microelectronics, protective coatings, and catalysis applications. For example, aluminum oxide thin films have a large band gap (7 eV),[1] low-leakage current densities (<2 MV cm^{-1}),[2−4] and a moderate dielectric constant (11),[2,3] which makes them excellent gate dielectric components in thin-film transistors (TFTs).[5−8] For this application, amorphous aluminum oxide thin films are preferred to avoid current leakage through crystalline grain boundaries.[9] However, the lack of long-range order in amorphous samples makes the study of structure−property relationships challenging.

Solid-state NMR (SSNMR) is a powerful tool for investigating both amorphous and crystalline materials because it is sensitive to short-range and long-range order. ^{27}Al SSNMR has previously been employed[10−20] to provide insight into the local structure of amorphous aluminum oxide thin films deposited from vapor-phase deposition methods.

Although traditional vapor-phase approaches produce high-quality aluminum oxide thin films, they generally involve expensive equipment and significant waste material. By contrast, solution deposition offers a cost-effective and scalable alternative, and solution-based routes to high-quality aluminum oxide films have been reported.[21−26] Here, we track the formation of aluminum oxide thin films deposited from aqueous aluminum precursors using high-field (19.96 T) ^{27}Al SSNMR in conjunction with conventional analysis techniques. Because local structure is likely very sensitive to deposition route and processing conditions, we have determined the evolution of aluminum site coordination from aqueous-derived

Received: December 5, 2017
Revised: October 7, 2018
Published: October 8, 2018

DOI: 10.1021/acs.chemmater.7b05078
Chem. Mater. 2018, 30, 7456−7463

aluminum oxide films and correlated the structure with film properties. Elucidating such relationships in solution-deposited films enables future development and optimization of solution deposition methods and provides insight into fundamental differences between solution- and vapor-deposited materials.

We also measure the dielectric response as a function of annealing temperature, which is affected by dehydration, decomposition of nitrate counterions, and the onset of crystallization of the aluminum oxide films. We relate the macroscopic polarizability (dielectric constant) of the films to the Al coordination, density, and crystallization. The local-structure/macroscopic property correlation provided by this study provides important insight into the chemical structures responsible for the observed electrical response.

EXPERIMENTAL SECTION

Preparation of Films. Aluminum oxide thin films were prepared by aqueous spin coating onto Si substrates. The precursor solution was prepared by electrolysis of an $Al(NO_3)_3$ solution, as described previously.[27] In summary, nitrate counterions were removed from a solution of $Al(NO_3)_3$ (Alfa Aesar, 98.0−102.0%) dissolved in 18.2 MΩ cm nanopure water into a fritted counter electrode compartment by passing 60 kC of reductive charge per mole $Al(NO_3)_3$ at a Pt working electrode placed in the main cell compartment. The reducing current drives the hydrogen evolution reaction, consuming protons in the main cell compartment while nitrates are driven across the frit into the counter electrode compartment (at which oxygen evolution occurs) to maintain charge balance.[27] The final precursor solution was diluted to 1 M [Al^{3+}] with a pH of 3. Liquid-state ^{27}Al NMR of the precursor (Figure S1, Supporting Information) shows a sharp peak at 0 ppm attributed to undistorted Al octahedra and a broader peak at 5 ppm consistent with distorted (often networked) Al octahedra. These two peaks are indicative of monomeric hexa-aqua ion $Al(H_2O)_6^{3+}$ and precondensed cluster species, such as $Al_{13}(OH)_{24}(H_2O)_{24}(NO_3)_{15}$.[28] Si substrates were cleaned in 1 M nitric acid (EMD, ACS grade) to remove any trace of adventitious Al-containing species, rinsed with 18.2 MΩ cm nanopure water, and treated in an O_2/N_2 plasma using a PE-50 Bench Plasma Cleaner (Plasma Etch, Inc.) set to maximum power. This surface treatment creates a hydrophilic surface, which is essential for uniform coverage of the deposited precursor solution.[29] Individual coats were deposited using 1 M (relative to Al^{3+}) solutions filtered through 0.2 μm poly(tetrafluoroethylene) syringe filters and spin-processed at 3000 rpm for 30 s. Films were promptly transferred to a hot plate set to 200 °C (in the case of the 200 °C sample) or 300 °C (for all other samples) and annealed for 15 min between coats. This process was repeated 10 times to generate thick (∼270 to 370 nm) films. A final 1 h anneal was performed in air at temperatures of 200, 300, 400, 500, 600, 700, 800, 950, or 1100 °C, using a hot plate or a box furnace.

Film Characterization. Films fabricated for X-ray diffraction (XRD) and Fourier transform infrared (FTIR) analysis were deposited onto high-resistivity IR-transparent double-sided-polished (100)-cut silicon wafers. XRD data were collected in grazing incidence XRD (GIXRD) geometry on a Rigaku SmartLab Diffractometer. The Cu source was held at 0.5° above the plane of the sample, and a 0 D scintillation detector was swept from 10° to 70° in 0.1° steps with a 12 s integration time per step. A single ten-coat film was annealed at 200 °C (as described above) and measured by GIXRD. The same film was then annealed to higher temperatures, increasing by 100 or 150 °C increments up to 1100 °C with GIXRD measurements at room temperature between each annealing step. FTIR analyses were performed on the same film after annealing at each temperature using a Thermo Fisher Nicolet 6700 FTIR spectrometer. Background corrections were made using a bare silicon substrate subjected to the same heat treatments.

Liquid-State NMR. The liquid-state ^{27}Al NMR spectrum was acquired using a 11.8-T magnet with a ^{27}Al Larmor frequency of 130.25 MHz using a Varian Unity Inova 500 MHz spectrometer. The aluminum precursor solution was placed into a 5 mm NMR tube, and the ^{27}Al spectrum was acquired using a Bloch decay pulse sequence with a recycle delay of 5 s (shown in Figure S1, Supporting Information). The spectrum was referenced to a 1.0 M solution of $Al(NO_3)_3$ in water.

Solid-State NMR. A series of aluminum oxide films were prepared for SSNMR analysis on 100 μm thick double-side-polished silicon wafers, as described previously. The aluminum oxide films (and silicon substrates) were crushed into a coarse powder using a mortar and pestle and packed into an NMR rotor. Solid-state ^{27}Al NMR spectra were acquired at 13.84 T corresponding to ^{27}Al Larmor frequencies of 153.69 MHz and were performed on a 2.5 mm HX MAS probe (with a low-aluminum background). All magic angle spinning (MAS) spectra were collected with a spinning frequency (ν_R) of 25 kHz. To ensure quantitative NMR spectra, a $\pi/18$ flip angle[30] was used in a Bloch decay experiment, with a pulse length of 0.34 μs. The recycle delay was 500 ms, and 100 800 transients were collected for each spectrum. Bloch decay spectra suffer from large background signals which were best addressed through a combination of deleting the first two points of the free induction decay, and implementation of a spline-fitting program (courtesy of Dr. Maxime Yon, CNRS) to reduce a "rolling baseline". The ^{27}Al background (from rotor and probe) was checked using identical experimental parameters on a KBr-filled rotor (for stability). No measurable background was found. All spectra were referenced to a 1.0 M solution of $Al(NO_3)_3$, and the NMR spectra were simulated using Dmfit.[31] (Additional NMR experiments performed, referred to in the Results and Discussion section, are described in the Supporting Information.)

The $^{[4]}Al$, $^{[5]}Al$, and $^{[6]}Al$ resonances were simulated using the "Czjzek" model[32−34] which accounts for the local structure of the aluminum sites arising from a statistical disorder of aluminum environments as observed in aluminum glasses and thin films.[15] The following parameters were allowed to fit within Dmfit to simulate the ^{27}Al NMR line shape: averaged isotropic chemical shift (δ_{ISO}), quadrupolar coupling constant (C_Q), amplitude, position, and width (for the Gaussian line shape). A value for "d" equal to 5 was used for the Czjzek model as any value outside of that is not physical in our system.[35] Note: During fitting of the line shape measured at 1100 °C, the peak representing $^{[5]}Al$ always converged to zero; hence, the concentration of the $^{[5]}Al$ was found to be 0 as seen in Figures 2 and 3.

Scanning Electron Microscopy and Ellipsometry. Aluminum oxide films were prepared for scanning electron microscopy (SEM) analysis by thermally evaporating ∼30 nm of Al onto the film surface. The Al metal top layer is deposited after annealing for SEM imaging purposes only. This step is necessary to prevent the accumulation of static electric charges ("charging") during SEM imaging.[9] Samples were then physically cleaved, and the corresponding cross sections were imaged using an FEI Helios Dual Beam SEM. Samples annealed >800 °C were imaged using a 3.0 keV accelerating voltage, while aluminum oxide samples annealed <700 °C required a lower accelerating voltage of 2.0 keV to limit beam damage to the films.

Film thicknesses were measured using a J.A. Woollam Co., Inc., EC-270 spectroscopic ellipsometer equipped with a LPS-400 75 W xenon light source and a M44 detector. To extract thickness values from raw ellipsometry data, a model using a single Cauchy layer, and a 1 mm Si substrate, was used. Initial best fits of the Cauchy layer were repeatedly perturbed and allowed to achieve new best fits, to ensure that the models did not settle on a local minimum.

Dielectric Constant Measurements. Dielectric constant measurements of aluminum oxide films were done asmetal−insulator−semiconductor (MIS) capacitors. 100 nm Al metal was deposited via thermal evaporation through a shadow mask onto annealed aluminum oxide films on top of a silicon substrate. Individual device areas were 0.011 cm^2. Device capacitance measurements were made via a Hewlett-Packard 4284a impedance analyzer at 20, 100, 1000, 10 000, and 100 000 Hz with a 50 mV oscillation amplitude.

DOI: 10.1021/acs.chemmater.7b05078
Chem. Mater. 2018, 30, 7456−7463

RESULTS AND DISCUSSION

Long-Range Structure. Figure 1 shows GIRXD patterns for aluminum oxide films annealed between 200 and 1100 °C.

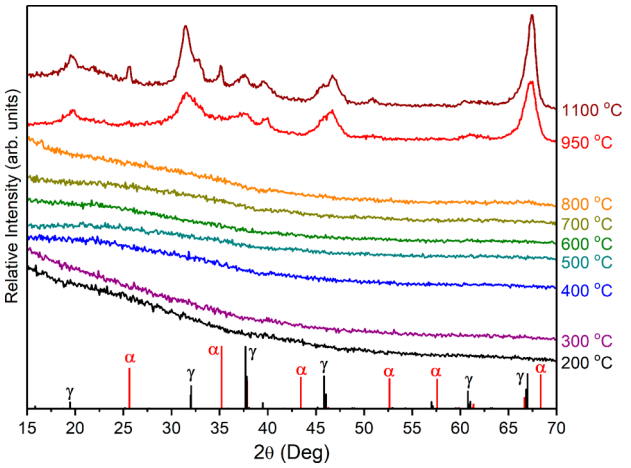

Figure 1. GIXRD patterns of aluminum oxide films sequentially annealed between 200 and 1100 °C. Peak positions for γ-Al_2O_3 (black, ICSD: 68771[39]) and α-Al_2O_3 (red, ICSD: 10425[36]) are shown for reference.

The absence of Bragg peaks for the films annealed between 200 and 800 °C suggests that the films are amorphous. Films annealed at 950 °C show Bragg diffraction peaks attributable to γ-Al_2O_3 and at 1100 °C to a mixture of α-Al_2O_3[36] and γ-Al_2O_3.[37] This conversion of γ-Al_2O_3 (and other low-temperature aluminum oxides) to α-Al_2O_3 at high temperatures has been observed previously.[37,38]

Local Structure. Solid-state ^{27}Al MAS NMR spectra were obtained for a separate set of aluminum oxide films annealed between 200 and 1100 °C. As a quadrupolar species, ^{27}Al has a nuclear spin quantum number, $I = {}^5/_2$. Figure 2 shows the solid-state NMR spectra collected at 13.84 T by Bloch decay. Such pulse-acquire sequences, with short excitation pulses,[30] are employed in an effort to obtain quantitative spectra.

The spectra were deconvoluted and fit to three ^{27}Al resonances using the Dmfit program.[31] The spectra are that of the central transition, and NMR resonances are similar to line shapes observed previously in crystalline-aluminum oxide,[40−45] thermally treated polyoxyaluminum clusters,[46] amorphous glasses,[31] chemical-vapor-deposited (CVD) aluminum oxide thin films,[15,18] and atomic layer deposited (ALD) alumina thin films.[11]

Similar to prior NMR studies of aluminum oxide films,[15] the "Czjzek" model, which accounts for the statistical disorder of aluminum environments that may be observed, was implemented within the Dmfit program.[32−34,47] The Czjzek model creates a joint probability distribution of the principal value V_{ZZ} of the diagonalized electric field gradient (EFG) tensor and of the quadrupolar asymmetry parameter η_Q, both of which impact the estimate of the diagonalized EFG tensor elements. The parameters used to simulate the NMR line shape include the averaged isotropic chemical shift (δ_{ISO}), chemical shift distribution (δ_{CS}), the averaged quadrupolar coupling constant (C_Q), and amplitude. These latter four parameters were allowed to optimize for each ^{27}Al resonance.

At this field, the $^{[4]}$Al, $^{[5]}$Al, and $^{[6]}$Al sites are reasonably resolved (Figure 2). $^{[n]}$Al represents the coordination number of the aluminum sites in the film, for example, $^{[6]}$Al represents an octahedral Al site. The films are composed of only these three types of aluminum coordination environments, as confirmed by 3QMAS (two-dimensional) ^{27}Al NMR,[48,49] shown in the Supporting Information, Figure S2. The 3QMAS spectrum was fit to provide good estimates of C_Q values for each of the sites, to help accurately deconvolute the one-dimensional ^{27}Al MAS (Bloch decay) NMR spectra. Such deconvolution permits the composition of the film to be determined, and these $^{[n]}$Al sites can be used to calculate an average coordination number, $\overline{CN}$, an approach used in other Al_xO_y studies.[15]

Figure 3 shows the relative ^{27}Al peak areas for $^{[4]}$Al, $^{[5]}$Al, and $^{[6]}$Al as a function of annealing temperature. The percentage of each $^{[n]}$Al was calculated from the Czjzek-optimized simulated fits, summarized in Table S1, Supporting

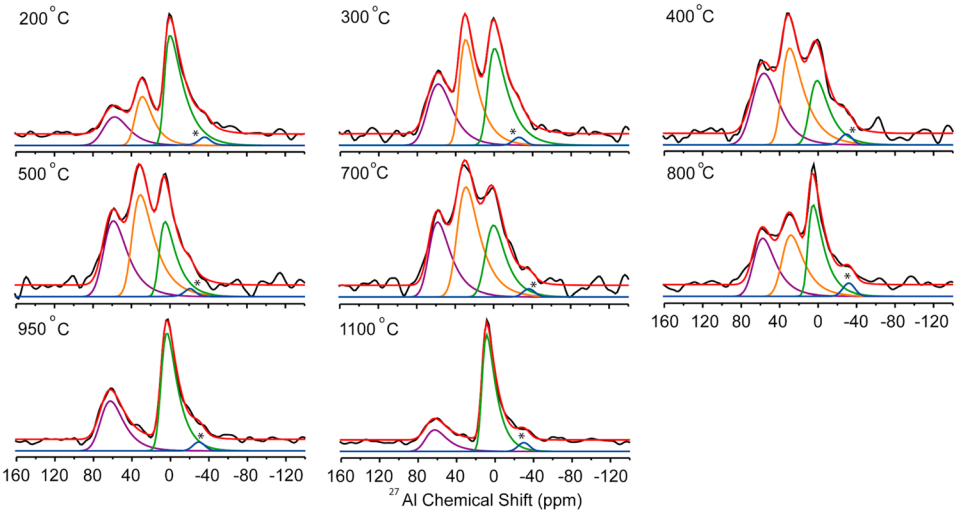

Figure 2. ^{27}Al MAS solid-state NMR spectra at 13.84 T of the central transitions of the aluminum oxide thin films annealed at temperatures indicated (200−1100 °C). The NMR line shapes have been deconvoluted into the individual Al coordination ($^{[n]}$Al) environments shown as purple ($^{[4]}$Al), orange ($^{[5]}$Al), and green ($^{[6]}$Al) line shapes, and the sum of the NMR resonances is shown in red. The * marks a spinning sideband from a satellite transition. The data have been normalized to the highest intensity peak.

DOI: 10.1021/acs.chemmater.7b05078
Chem. Mater. 2018, 30, 7456−7463

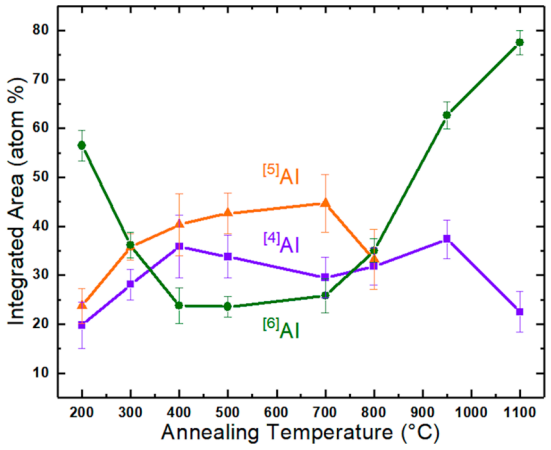

Figure 3. Plot of peak areas for each Al coordination versus annealing temperature from ^{27}Al SSNMR data of Figure 2. The integrated area of the deconvoluted ^{27}Al NMR resonances are $^{[4]}$Al (purple squares), $^{[5]}$Al (orange triangles), and $^{[6]}$Al (green circles).

Information. A full table of parameters used in the Dmfit simulations are provided in Table S2.

The spectra for the two highest temperature films are composed of only $^{[4]}$Al and $^{[6]}$Al sites, which is consistent with the structure of γ-Al_2O_3 revealed by the GIXRD data and ^{27}Al NMR of γ-Al_2O_3[50] (noting that α-Al_2O_3 displays only $^{[6]}$Al sites).[51] At lower annealing temperatures, where GIXRD indicates that the films are amorphous, the NMR spectra show all three coordination environments ($^{[4]}$Al, $^{[5]}$Al, and $^{[6]}$Al).

Morphology. Figure 4 shows cross-sectional SEM images for films annealed at 300, 800, 950, and 1100 °C. The Si

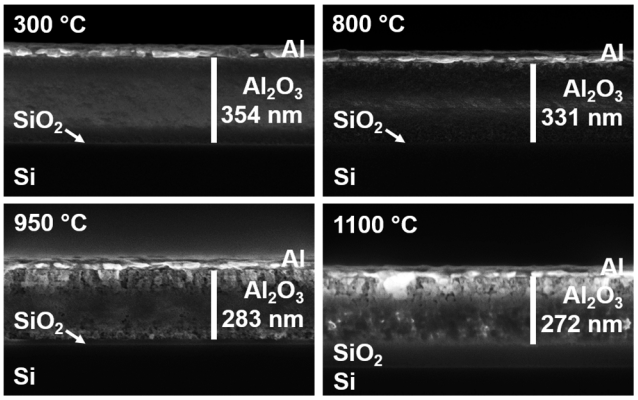

Figure 4. Cross-sectional SEM images of aluminum oxide films prepared at 300, 800, 950, and 1100 °C. A full series of SEM images may be found in Figure S3.

substrate is also evident, including a thin layer of native SiO_2. The smooth film/Al top-coat interface at 300 and 800 °C is consistent with an amorphous film. The morphology of the film changes with annealing temperature, as evidenced by the texture that develops near the film surface and the film/SiO_2 interface at 950 °C, then throughout the film at 1100 °C. This texture implies the growth of crystalline phases of aluminum oxide, consistent with GIXRD and NMR data. Additionally, the SiO_2 layer grows to approximately 20 nm at 950 °C and further to 90 nm at 1100 °C, which is consistent with reports of thermally grown SiO_2.[2,52,53] Figure S3 presents a full series of SEM images for films annealed between 300 and 1100 °C.

Chemical Evolution. Figure 5 shows FTIR spectra of the thin films annealed from 200 to 1100 °C (as labeled). The

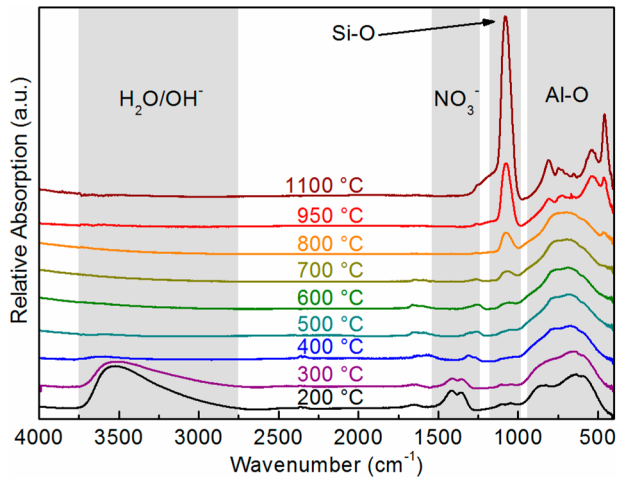

Figure 5. FTIR spectra of the thin films annealed from 200 to 1100 °C.

most discernible difference in the spectra is the loss of the hydroxyl (O−H) stretching vibration at 3500 cm^{-1}.[25] The water (O−H) stretching mode decreases substantially by 400 °C, revealing that most residual water and hydroxides are removed from the film at this temperature (limited by the detection sensitivity of the IR experiment for the O−H stretch). Temperature-programmed desorption (TPD) indicates −OH persists in the films to temperatures as high as 700 °C, Figure S4. The nitrate (N−O) vibrational modes at 1420 and 1360 cm^{-1} follow a similar trend, indicating the loss of nitrate counterions by 400 °C.[54] The modes between 400 and 900 cm^{-1} are commonly attributed to the aluminum oxide (Al−O) stretching vibrations, and these modes sharpen at the higher temperatures where α- and γ-Al_2O_3 crystallize.[55,56] The modes at 1600 cm^{-1} are H_2O rocking vibrations from bound waters.[55] The peak at 1240 cm^{-1} corresponds to Si−O−Si vibrations; this mode increases in intensity with increasing temperature consistent with SiO_2 growth. Such an interfacial silicon dioxide layer grows between the silicon substrate and the thin film,[2,52,53] which agrees with the cross-sectional SEM (Figure 4 and Figure S3).

Aggregate Analysis of Film Evolution. Considering the local, chemical, and structural information together, a picture emerges for which three distinct temperature "regions" can be discerned as the amorphous aluminum oxide films are heated. The first region is in the annealing temperature range between 200 and 400 °C (from Figure 3). The precursor contains Al exclusively as $^{[6]}$Al. After spin coating and annealing at 200 °C, 40% of $^{[6]}$Al has converted to $^{[5]}$Al and $^{[4]}$Al. This conversion continues with further heating, as only 20−25% of the $^{[6]}$Al sites remain at 400 °C. These results, considered in the context of the IR and TPD measurements, suggest that the loss of H_2O leads to a decrease in the Al coordination such that the $^{[6]}$Al sites with H_2O or hydroxide ligands convert to $^{[4]}$Al and $^{[5]}$Al species. Scheme 1 depicts three likely reactions that result in the release of water and a decrease in coordination number. Reaction 1 shows the release of a ligating H_2O, and reactions 2 and 3 show condensation with formation of a bridging oxide species. The difference between the two is the coordination of the initial ligands. When two bridging hydroxides are replaced

DOI: 10.1021/acs.chemmater.7b05078
Chem. Mater. 2018, 30, 7456−7463

Scheme 1

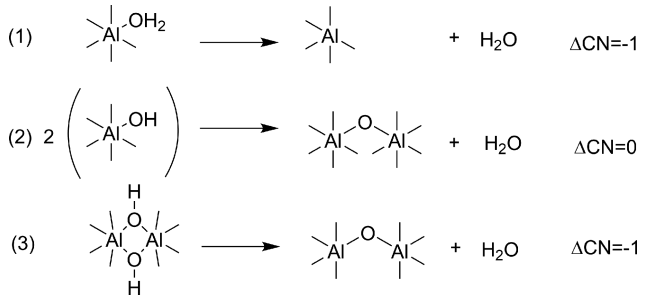

with a bridging oxide, the coordination of each Al decreases by one.

The second region of interest is the annealing temperature range from 400 to 700 °C. In this region the Al coordination numbers are essentially static. The films remain amorphous, and FTIR spectra exhibit only modest changes.

Films annealed to temperatures >700 °C begin to exhibit changes in film structure. GIXRD patterns indicate that crystalline phases of γ- and α-Al_2O_3 form in the films >800 °C. These data are corroborated by the SSNMR spectra, where the $^{[5]}$Al site intensity decreases and disappears, and $^{[6]}$Al becomes the dominant coordination environment. Pure α-Al_2O_3 would be entirely $^{[6]}$Al,[40,43,44] while pure γ-Al_2O_3 is a mix of $^{[4]}$Al and $^{[6]}$Al.[44,57,58] A slight shift of the $^{[6]}$Al resonance is found with annealing temperature, even at 950 to 1100 °C, consistent with the beginning of formation of α-Al_2O_3. The cross-sectional SEM images corroborate that crystallization occurs in this region. The presence of sharp aluminum oxide (Al−O) stretching vibrations (between 400−900 cm^{-1}) in the FTIR spectra are also consistent with crystalline structures.[55,56]

Overall, our results suggest constitutional water loss and dehydroxylation lead to an initial predominance of $^{[5]}$Al and $^{[4]}$Al sites in the spin-coated aluminum oxide films. The presence of −OH in nanopores within the film likely pins and stabilizes the amorphous structure at high temperatures. As pore-based −OH is released, the film begins to further densify and crystallize as the α and γ morphs of Al_2O_3.

Solution Deposition and MOCVD. The quantitative veracity of NMR has been well established for crystalline- and porous-aluminum oxides;[59] Samain, Jaworski, and Edén et al. have demonstrated that porous γ-Al_2O_3 contains tetrahedral Al and octahedral Al sites in relative amounts of 0.3 and 0.7, respectively.[58] The 1100 °C film in this study most closely identifies to the crystalline phase of γ-Al_2O_3 with $^{[4]}$Al and $^{[6]}$Al present at amounts of 0.22 and 0.78, respectively. Sarou-Kanian, Gleizes, and Florian et al.[15] describe the MOCVD film annealed at 720 °C as containing nanocrystals of γ-Al_2O_3 in the film; however, a full transition to γ-Al_2O_3 is not seen in Sarou-Kanian's study.

The coordination environment of Al in amorphous aluminum oxide thin films deposited by MOCVD has previously been investigated via SSNMR by Sarou-Kanian, Gleizes, and Florian et al.[15] In the study, the effect of varying substrate temperature during deposition is examined. Figure 6 shows the average Al coordination number, $\overline{CN}$, as a function of anneal temperature. $\overline{CN}$ is calculated using the peak areas, as shown in eq 1.[15]

$$\overline{CN} = \frac{[(\%^{[4]}\mathrm{Al})\cdot 4] + [(\%^{[5]}\mathrm{Al})\cdot 5)] + [(\%^{[6]}\mathrm{Al})\cdot 6]}{100} \quad (1)$$

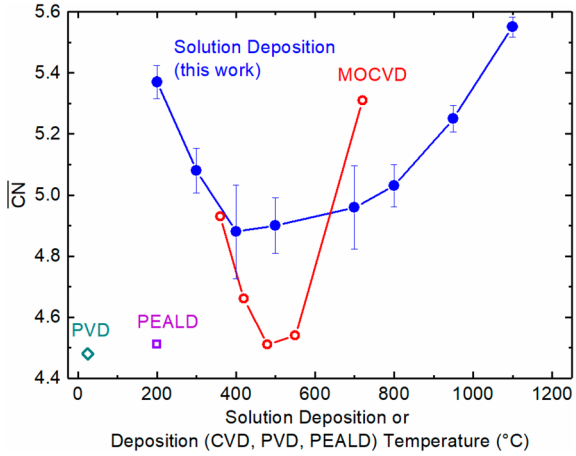

Figure 6. Average coordination ($\overline{CN}$) of aluminum in aluminum oxide thin films deposited by solution and MOCVD techniques and then annealed at selected temperatures.[11,14,15]

Qualitatively, the $\overline{CN}$s of Al in the MOCVD and solution-deposited aluminum oxide are similar: an initial high value at low temperatures followed by a decrease at intermediate temperatures and an increase at higher temperatures (presumably upon crystallization).[14] There are two notable differences between the plots of the average coordination environment versus temperature. In a comparision of the two deposition methods in more detail, the onset temperature at which $\overline{CN}$ increases rapidly and crystallization becomes evident is >800 °C for solution deposition, while at a lower temperature (>550 °C) for MOCVD. Solution deposition results in a film that retains a disordered structure until a much higher temperature. In addition, the average coordination number is overall a bit higher for solution deposition, with a larger fraction of $^{[6]}$Al sites compared to that found for MOCVD. We propose that these temperatures reflect both the deposition methods and the film compositions. The MOCVD films are reported to be largely dehydroxylated at temperatures above 415 °C. In MOCVD, deposition is a continuous growth process wherein decomposition of aluminum tri-isopropoxide occurs at the surface of the heated substrate and growing film.[50] This surface-mediated decomposition limits hydroxide formation. The solution process deposits the aqueous aluminum precursor followed by an anneal to remove water, hydroxide, and nitrate. All of the material is deposited prior to heating; thus, the activation energies for bulk diffusion[51] in the film must be overcome to desorb constituents and induce crystallization. Consequently, the MOCVD and solution-deposited films form chemically distinct amorphous structures along their pathways to crystalline Al_2O_3 films.

Dielectric Response and Film Structure. Film structure provides a key element to understanding film properties and for tuning future syntheses for desired functions. One such property is the dielectric constant. The aluminum oxide thin films examined in this study exhibit dielectric constants that range from 6 to 11. This large range arises from changes in chemical, local, and long-range structures.

Figure 7 depicts changes in the film's dielectric response concomitant with changes in $^{[6]}$Al percentage and H_2O and nitrate IR intensities. In the region 200−400 °C, the film exhibits a decrease in the dielectric constant from ≈11 (200 °C) to ≈6 (400 °C) (see also Figure S5). From measurements on the frequency dependence of the dielectric response (Figure

DOI: 10.1021/acs.chemmater.7b05078
Chem. Mater. 2018, 30, 7456−7463

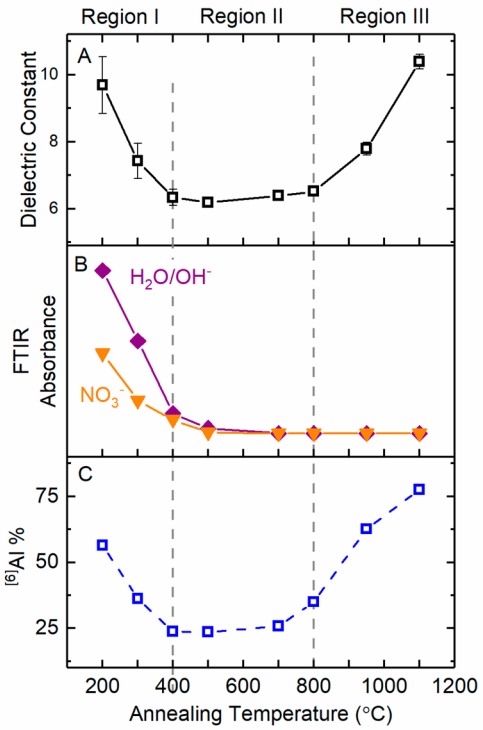

Figure 7. (A) Dielectric constant at 10 kHz, (B) FTIR absorbance of O−H and O−N stretching modes, and (C) $^{[6]}$Al content of films (from ^{27}Al NMR) vs annealing temperature. The frequency dependence of the dielectric constant at different annealing temperatures is presented in Figure S5.

S5), the films annealed at low temperatures exhibit a higher dielectric constant at lower frequency because of substantial ionic and vibrational contributions that are absent at high frequency. This decrease in the dielectric constant may be due to elimination of residual water, hydroxides, and nitrates in the films (as observed by FTIR), creating a less polarizable film. As the films are annealed from 400 to 800 °C, the dielectric constant is largely unaffected (shown by the frequency dependence of the dielectric constant). Similarly, the $^{[6]}$Al content does not change over this temperature range. The ≈10−15% increase in the $^{[6]}$Al (at the expense of the $^{[5]}$Al species) from 400 to 800 °C appears to have no effect on the dielectric constant.

When the films start to crystallize (>800 °C), the dielectric constant increases from 6.5 to 10.4. This increase correlates with increased $^{[6]}$Al concentration, which can be due to the increased polarizability of O with the longer Al−O distances associated with the higher coordination numbers. The films also densify and crystallize in this region, which should also increase the dielectric constant. Densification of the film increases the density of polarizable electrons that contribute to the dielectric constant. The frequency response of the dielectric constant (Figure S5) confirms that at high annealing temperatures the dielectric constant has no dependence on the frequency; thus, there are minimal contributions from ionic polarization. Densification of the film is a consequence of the conversion of $^{[4]}$Al and $^{[5]}$Al to $^{[6]}$Al sites.[60] The end point of this temperature range is where γ-Al_2O_3 appears, which has a less open network and a higher density than the amorphous film.

Once the film has been annealed at 1100 °C, diffraction shows the structure is a mixture of γ-Al_2O_3 and α-Al_2O_3 (Figure 1). The dielectric constant increases by 33% at this high temperature to a value of ∼10.5. SSNMR shows a small change in the amount of $^{[6]}$Al for the samples annealed at 950 and 1100 °C. α-Al_2O_3 is known to have an anisotropic dielectric constant with respect to its unit cell; thus, the texture of the α-Al_2O_3 crystallites can have a dramatic effect on the measured dielectric constant in the out-of-plane direction (normal to the direction of growth).[61] It is possible that the presence of α-Al_2O_3 at 1100 °C is the cause of the increase in the dielectric constant beyond densification alone.

CONCLUSION

We have investigated the evolution of aqueous aluminum solution precursors from an amorphous to crystalline Al_2O_3 thin film. The structural changes were monitored by ^{27}Al solid-state NMR combined with FTIR and GIXRD, showing speciation of four-, five-, and six-coordinate Al sites. We have determined that the aluminum oxide films do not reach a steady amorphous structure until the majority of H_2O, NO_3^-, and OH^- ligands have decomposed (by 400 °C). The amorphous structures formed by solution processing at temperatures above 400 °C may differ substantively from those of amorphous aluminum oxide thin films deposited by MOCVD. Finally, as H_2O/OH^- and NO_3^- are released from the film, we observe changes in the dielectric constant that correlate strongly with the SSNMR measurements, following both the trend of $\overline{CN}$ and the fraction of $^{[6]}$Al in each spectrum. This study provides a window into the process by which aqueous aluminum precursors evolve into extended oxide networks. Additionally, we demonstrate that aqueous-derived aluminum oxide films exhibit structural conversions between four-, five-, and six-coordinate ^{27}Al sites that evolve as a function of annealing temperature with an onset of crystallization at a higher temperature than other routes.

ASSOCIATED CONTENT

Supporting Information

The Supporting Information is available free of charge on the ACS Publications website at DOI: 10.1021/acs.chemmater.7b05078.

Liquid-state ^{27}Al NMR of the aqueous aluminum precursor, ^{27}Al 3QMAS NMR of a 300 °C film, SEM images of amorphous aluminum oxide films, temperature-programmed desorption data for multiple films, frequency dependence of the dielectric constant, ^{27}Al solid-state MAS NMR with a wider spectral window (from that depicted in Figure 2) is shown after processing with the spline-fitting program, and tables of deconvoluted ^{27}Al NMR data and Dmfit fitting parameters are provided (PDF)

AUTHOR INFORMATION

Corresponding Authors

*E-mail: hayes@wustl.edu.
*E-mail: cpage@uoregon.edu.
*E-mail: swb@uoregon.edu.

ORCID

Jinlei Cui: 0000-0002-9304-4330
Matthew G. Kast: 0000-0003-2482-113X

DOI: 10.1021/acs.chemmater.7b05078
Chem. Mater. 2018, 30, 7456−7463

Blake A. Hammann: 0000-0003-2972-091X
Cory K. Perkins: 0000-0002-5098-0217
Douglas A. Keszler: 0000-0002-7112-1171
Catherine J. Page: 0000-0002-4545-7835
Shannon W. Boettcher: 0000-0001-8971-9123
Sophia E. Hayes: 0000-0002-2809-6193

Author Contributions

#These authors (J.C. and M.G.K.) contributed equally to this work. The manuscript was written through contributions of all authors. All authors have given approval to the final version of the manuscript.

Notes

The authors declare no competing financial interest.

■ ACKNOWLEDGMENTS

This material is based on work in the Center for Sustainable Materials Chemistry, which is supported by the U.S. National Science Foundation under Grant CHE-1606982. The authors thank Dr. Athavan Nadarajah, Dr. Juan Carlos Ramos, and Dr. Deok-Hie Park for helpful discussions. High-field 3QMAS NMR was performed at the National High Magnetic Field Laboratory in Tallahassee, FL, which is supported by the NSF (DMR-1644779) and by the State of Florida, with assistance from Drs. Zhehong Gan and Ivan Hung.

■ REFERENCES

(1) Filatova, E. O.; Konashuk, A. S. Interpretation of the Changing the Band Gap of Al_2O_3 Depending on Its Crystalline Form: Connection with Different Local Symmetries. *J. Phys. Chem. C* **2015**, *119*, 20755−20761.
(2) Smith, S. W.; Wang, W.; Keszler, D. A.; Conley, J. F. Solution Based Prompt Inorganic Condensation and Atomic Layer Deposition of Al_2O_3 Films: A Side-by-Side Comparison. *J. Vac. Sci. Technol., A* **2014**, *32*, 041501.
(3) DaSilva, E. M.; White, P. Electrical Properties of Evaporated Molybdenum Oxide Films. *J. Electrochem. Soc.* **1962**, *109*, 12−15.
(4) Wang, W.; Keszler, D. A. Process to Form Aqueous Precursor and Aluminum Oxide Film. U.S. Patent 9340678B2, 2016.
(5) Kim, J. B.; Fuentes-Hernandez, C.; Potscavage, W. J.; Zhang, X.-H.; Kippelen, B. Low-Voltage InGaZnO Thin-Film Transistors with Al_2O_3 Gate Insulator Grown by Atomic Layer Deposition. *Appl. Phys. Lett.* **2009**, *94*, 142107.
(6) Lim, S. J.; Kwon, S. J.; Kim, H.; Park, J. S. High Performance Thin Film Transistor with Low Temperature Atomic Layer Deposition Nitrogen-Doped ZnO. *Appl. Phys. Lett.* **2007**, *91*, 183517.
(7) Park, J. S.; Maeng, W. J.; Kim, H. S.; Park, J. S. Review of Recent Developments in Amorphous Oxide Semiconductor Thin-Film Transistor Devices. *Thin Solid Films* **2012**, *520*, 1679−1693.
(8) Fortunato, E.; Barquinha, P.; Martins, R. Oxide Semiconductor Thin-Film Transistors: A Review of Recent Advances. *Adv. Mater.* **2012**, *24*, 2945−2986.
(9) Jiang, K.; Anderson, J. T.; Hoshino, K.; Li, D.; Wager, J. F.; Keszler, D. A. Low-Energy Path to Dense HfO_2 Thin Films with Aqueous Precursor. *Chem. Mater.* **2011**, *23* (13), 945−952.
(10) Dupree, R.; Farnan, I.; Forty, A. J.; El-Mashri, S.; Bottyan, L. A MAS NMR Study of the Structure of Amorphous Alumina Films. *J. Phys. Colloques* **1985**, *46* (C8), C8-113−C8-117.
(11) Lee, S. K.; Park, S. Y.; Yi, Y. S.; Moon, J. Structure and Disorder in Amorphous Alumina Thin Films: Insights from High-Resolution Solid-State NMR. *J. Phys. Chem. C* **2010**, *114*, 13890−13894.
(12) Kim, H. J.; Lee, H. C.; Lee, J. S. ^{27}Al Triple-Quantum Magic-Angle Spinning Nuclear Magnetic Resonance Characterization of Nanostructured Alumina Materials. *J. Phys. Chem. C* **2007**, *111*, 1579−1583.
(13) Lee, S. K.; Ahn, C. W. Probing of 2 Dimensional Confinement-Induced Structural Transitions in Amorphous Oxide Thin Film. *Sci. Rep.* **2015**, *4*, 4200.
(14) Lee, S. K.; Park, S. Y.; Yi, Y. S.; Ahn, C. W.; Lee, S. B. Structure of Amorphous Aluminum Oxide. *Phys. Rev. Lett.* **2009**, *103*, 095501.
(15) Sarou-Kanian, V.; Gleizes, A. N.; Florian, P.; Samélor, D.; Massiot, D.; Vahlas, C. Temperature-Dependent 4-, 5- and 6-Fold Coordination of Aluminum in MOCVD-Grown Amorphous Alumina Films: A Very High Field ^{27}Al-NMR Study. *J. Phys. Chem. C* **2013**, *117*, 21965−21971.
(16) Kim, N.; Bassiri, R.; Fejer, M. M.; Stebbins, J. F. The Structure of Ion Beam Sputtered Amorphous Alumina Films and Effects of Zn Doping: High-Resolution ^{27}Al NMR. *J. Non-Cryst. Solids* **2014**, *405*, 1−6.
(17) Nayar, B. C. P.; Khanna, A.; Kabiraj, D.; Abhilash, S. R.; Beake, B. D.; Losset, Y.; Chen, B. Structural, Optical and Mechanical Properties of Amorphous and Crystalline Alumina Thin Films. *Thin Solid Films* **2014**, *568*, 19−24.
(18) Baggetto, L.; Sarou-Kanian, V.; Florian, P.; Gleizes, A. N.; Massiot, D.; Vahlas, C. Atomic Scale Structure of Amorphous Aluminum Oxyhydroxide, Oxide and Oxycarbide Films Probed by Very High Field ^{27}Al Nuclear Magnetic Resonance. *Phys. Chem. Chem. Phys.* **2017**, *19*, 8101−8110.
(19) Zhang, L.; de Araujo, C. C.; Eckert, H. Aluminum Lactate - An Attractive Precursor for Sol-Gel Synthesis of Alumina-Based Glasses. *J. Non-Cryst. Solids* **2007**, *353*, 1255−1260.
(20) Lee, S. K.; Ryu, S. Probing of Triply Coordinated Oxygen in Amorphous Al_2O_3. *J. Phys. Chem. Lett.* **2018**, *9*, 150−156.
(21) Kast, M. G.; Cochran, E. A.; Enman, L. J.; Mitchson, G.; Siefe, C.; Plassmeyer, P. N.; Greenaway, A. L.; Johnson, D. C.; Page, C. J.; Boettcher, S. W. Amorphous Mixed-Metal Oxide Thin Films from Aqueous Solution Precursors with Near-Atomic Smoothness. *J. Am. Chem. Soc.* **2016**, *138*, 16800−16808.
(22) Woods, K. N.; Waddington, E. C.; Crump, C. A.; Bryan, E. A.; Gleckler, T. S.; Nellist, M. R.; Duell, B. A.; Nguyen, D. P.; Boettcher, S. W.; Page, C. J. Tunable High-κ $Zr_xAl_{1-x}O_y$ Thin Film Dielectrics from All-Inorganic Aqueous Precursor Solutions. *RSC Adv.* **2017**, *7*, 39147−39152.
(23) Huang, G.; Duan, L.; Dong, G.; Zhang, D.; Qiu, Y. High-Mobility Solution-Processed Tin Oxide Thin-Film Transistors with High - κ Alumina Dielectric Working in Enhancement Mode. *ACS Appl. Mater. Interfaces* **2014**, *6*, 20786−20794.
(24) Liu, A.; Liu, G.; Zhu, H.; Shin, B.; Fortunato, E.; Martins, R.; Shan, F. Eco-Friendly Water-Induced Aluminum Oxide Dielectrics and Their Application in a Hybrid Metal Oxide/Polymer TFT. *RSC Adv.* **2015**, *5*, 86606−86613.
(25) Xu, W.; Wang, H.; Xie, F.; Chen, J.; Cao, H.; Xu, J.-B. Facile and Environmentally Friendly Solution-Processed Aluminum Oxide Dielectric for Low-Temperature, High-Performance Oxide Thin-Film Transistors. *ACS Appl. Mater. Interfaces* **2015**, *7*, 5803−5810.
(26) Rim, Y. S.; Chen, H.; Song, T. B.; Bae, S. H.; Yang, Y. Hexaaqua Metal Complexes for Low-Temperature Formation of Fully Metal Oxide Thin-Film Transistors. *Chem. Mater.* **2015**, *27*, 5808−5812.
(27) Wang, W.; Liu, W.; Chang, I.-Y.; Wills, L. A.; Zakharov, L. N.; Boettcher, S. W.; Cheong, P. H.-Y.; Fang, C.; Keszler, D. A. Electrolytic Synthesis of Aqueous Aluminum Nanoclusters and in Situ Characterization by Femtosecond Raman Spectroscopy and Computations. *Proc. Natl. Acad. Sci. U. S. A.* **2013**, *110*, 18397−18401.
(28) Wang, W. *Synthesis and Characterization of Aluminum Oxide Based Materials - from Molecule to Device*. Ph.D. Thesis, Oregon State University, 2013.
(29) Cong, C.; Li, K.; Zhang, X. X.; Yu, T. Visualization of Arrangements of Carbon Atoms in Graphene Layers by Raman Mapping and Atomic-Resolution TEM. *Sci. Rep.* **2013**, *3*, 1195.
(30) Lippmaa, E.; Samoson, A.; Magi, M. High-Resolution Aluminum-27 NMR of Aluminosilicates. *J. Am. Chem. Soc.* **1986**, *108*, 1730−1735.

DOI: 10.1021/acs.chemmater.7b05078
Chem. Mater. 2018, 30, 7456−7463

(31) Massiot, D.; Fayon, F.; Capron, M.; King, I.; Le Calvé, S.; Alonso, B.; Durand, J. O.; Bujoli, B.; Gan, Z.; Hoatson, G. Modelling One- and Two-Dimensional Solid-State NMR Spectra. *Magn. Reson. Chem.* **2002**, *40*, 70−76.
(32) Czjzek, G.; Fink, J.; Gotz, F.; Schmidt, H.; Coey, J. M. D.; Rebouillat, J.-P.; Lienard, A. Atomic Coordination and the Distribution of Electric Field Gradients in Amorphous Solids. *Phys. Rev. B: Condens. Matter Mater. Phys.* **1981**, *23*, 2513−2530.
(33) d'Espinose de Lacaillerie, J. B.; Fretigny, C.; Massiot, D. MAS NMR Spectra of Quadrupolar Nuclei in Disordered Solids: The Czjzek Model. *J. Magn. Reson.* **2008**, *192*, 244−251.
(34) Le Caër, G.; Bureau, B.; Massiot, D. An Extension of the Czjzek Model for the Distributions of Electric Field Gradients in Disordered Solids and an Application to NMR Spectra of ^{71}Ga in Chalcogenide Glasses. *J. Phys.: Condens. Matter* **2010**, *22*, 065402.
(35) Neuville, D. R.; Cormier, L.; Massiot, D. Al Environment in Tectosilicate and Peraluminous Glasses: A ^{27}Al MQ-MAS NMR, Raman, and XANES Investigation. *Geochim. Cosmochim. Acta* **2004**, *68*, 5071−5079.
(36) Ishizawa, N.; Miyata, T.; Minato, I.; Marumo, F.; Iwai, S. A Structural Investigation of α- Al_2O_3 at 2170 K. *Acta Crystallogr., Sect. B: Struct. Crystallogr. Cryst. Chem.* **1980**, *36*, 228−230.
(37) Repelin, Y.; Husson, E. Etudes Structurales d'alumines de Transition. I-Alumines Gamma et Delta. *Mater. Res. Bull.* **1990**, *25*, 611−621.
(38) Wefers, K.; Misra, C. Oxides and Hydroxides of Aluminum. *Alcoa Technical Paper Number 19; Alcoa Labs, Alcoa Center, PA (1987);* **1987**, 47.
(39) Li, D.-L.; O'Connor, B. H.; Roach, G. I. D.; Cornell, J. B. Structural Models of Eta- and Gamma-Aluminas by X-Ray Rietveld Refinement. *Acta Crystallogr. Sect. A Found. Crystallogr.* **1990**, *46*, C61.
(40) O'Dell, L. A.; Savin, S. L. P.; Chadwick, A. V.; Smith, M. E. A 27Al MAS NMR Study of a Sol-Gel Produced Alumina: Identification of the NMR Parameters of the θ- Al_2O_3 Transition Alumina Phase. *Solid State Nucl. Magn. Reson.* **2007**, *31*, 169−173.
(41) Wischert, R.; Florian, P.; Copéret, C.; Massiot, D.; Sautet, P. Visibility of Al Surface Sites of γ-Alumina: A Combined Computational and Experimental Point of View. *J. Phys. Chem. C* **2014**, *118*, 15292−15299.
(42) Pecharromán, C.; Sobrados, I.; Iglesias, J. E.; González-Carreño, T.; Sanz, J. Thermal Evolution of Transitional Aluminas Followed by NMR and IR Spectroscopies. *J. Phys. Chem. B* **1999**, *103*, 6160−6170.
(43) Lee, M. H.; Cheng, C. F.; Heine, V.; Klinowski, J. Distribution of Tetrahedral and Octahedral Al Sites in Gamma Alumina. *Chem. Phys. Lett.* **1997**, *265*, 673−676.
(44) Fitzgerald, J. J.; Piedra, G.; Dec, S. F.; Seger, M.; Maciel, G. E. Dehydration Studies of a High-Surface-Area Alumina (Pseudo-Boehmite) Using Solid-State ^{1}H and ^{27}Al NMR. *J. Am. Chem. Soc.* **1997**, *119*, 7832−7842.
(45) Wang, J. A.; Bokhimi, X.; Morales, A.; Novaro, O.; López, T.; Gómez, R. Aluminum Local Environment and Defects in the Crystalline Structure of Sol−Gel Alumina Catalyst. *J. Phys. Chem. B* **1999**, *103*, 299−303.
(46) Nazar, L. F.; Fu, G.; Bain, A. D. ^{27}Al MAS NMR Studies of a New Polyoxyaluminium Cluster and Its Selective Transformation to Five-Coordinate Aluminium in the Solid State. *J. Chem. Soc., Chem. Commun.* **1992**, No. 3, 251−253.
(47) Wang, X.; Guo, Y.; Lu, G.; Hu, Y.; Jiang, L.; Guo, Y.; Zhang, Z. An Excellent Support of Pd Catalyst for Methane Combustion: Thermal-Stable Si-Doped Alumina. *Catal. Today* **2007**, *126*, 369−374.
(48) Gleizes, A. N.; Samélor, D.; Vahlas, C.; Sarou-Kanian, V.; Florian, P.; Massiot, D. Temperature Dependent 4-, 5- and 6-Fold Coordination of Aluminum in MOCVD-Grown Amorphous Alumina Films: From Local Coordination to Material Properties. *Adv. Sci. Technol.* **2014**, *91*, 123−133.
(49) Hung, I.; Trébosc, J.; Hoatson, G. L.; Vold, R. L.; Amoureux, J. P.; Gan, Z. Q-Shear Transformation for MQMAS and STMAS NMR Spectra. *J. Magn. Reson.* **2009**, *201*, 81−86.
(50) Kwak, J. H.; Hu, J. Z.; Kim, D. H.; Szanyi, J.; Peden, C. H. F. Penta-Coordinated Al^{3+} Ions as Preferential Nucleation Sites for BaO on γ - Al_2O_3: An Ultra-High-Magnetic Field ^{27}Al MAS NMR Study. *J. Catal.* **2007**, *251*, 189−194.
(51) Sabarinathan, V.; Ramasamy, S.; Ganapathy, S. Perturbations to ^{27}Al Electric Field Gradients in Nanocrystalline α - Al_2O_3 Studied by High-Resolution Solid-State NMR. *J. Phys. Chem. B* **2010**, *114*, 1775−1781.
(52) Rouchon, D.; Rochat, N.; Gustavo, F.; Chabli, a.; Renault, O.; Besson, P. Study of Ultrathin Silicon Oxide Films by FTIR-ATR and ARXPS after Wet Chemical Cleaning Processes. *Surf. Interface Anal.* **2002**, *34*, 445−450.
(53) Tian, R.; Seitz, O.; Li, M.; Hu, W.; Chabal, Y. J.; Gao, J. Infrared Characterization of Interfacial Si−O Bond Formation on Silanized Flat SiO_2/Si Surfaces. *Langmuir* **2010**, *26*, 4563−4566.
(54) Park, J. H.; Kim, K.; Yoo, Y. B.; Park, S. Y.; Lim, K.-H.; Lee, K. H.; Baik, H. K.; Kim, Y. S. Water Adsorption Effects of Nitrate Ion Coordinated Al_2O_3 Dielectric for High Performance Metal-Oxide Thin-Film Transistor. *J. Mater. Chem. C* **2013**, *1*, 7166−7174.
(55) Ozer, N.; Cronin, J.; Yao, Y.-J.; Tomsia, A. P. Optical Properties of Sol-Gel Deposited Al_2O_3 Films. *Sol. Energy Mater. Sol. Cells* **1999**, *59*, 355−366.
(56) Shamala, K. S.; Murthy, L. C. S.; Narasimha Rao, K. Studies on Optical and Dielectric Properties of Al_2O_3 Thin Films Prepared by Electron Beam Evaporation and Spray Pyrolysis Method. *Mater. Sci. Eng., B* **2004**, *106*, 269−274.
(57) Damodaran, K.; Rajamohanan, P. R.; Chakrabarty, D.; Racherla, U. S.; Manohar, V.; Fernandez, C.; Amoureux, J. P.; Ganapathy, S. Triple-Quantum Magic Angle Spinning ^{27}Al NMR of Aluminum Hydroxides. *J. Am. Chem. Soc.* **2002**, *124*, 3200−3201.
(58) Samain, L.; Jaworski, A.; Edén, M.; Ladd, D. M.; Seo, D. K.; Javier Garcia-Garcia, F.; Häussermann, U. Structural Analysis of Highly Porous γ- Al_2O_3. *J. Solid State Chem.* **2014**, *217*, 1−8.
(59) Freude, D. Quadrupolar Nuclei in Solid-State Nuclear Magnetic Resonance. *Encycl. Anal. Chem.* **2006**, 12188−12224.
(60) Momida, H.; Hamada, T.; Takagi, Y.; Yamamoto, T.; Uda, T.; Ohno, T. Theoretical Study on Dielectric Response of Amorphous Alumina. *Phys. Rev. B: Condens. Matter Mater. Phys.* **2006**, *73*, 054108.
(61) Fontanella, J.; Andeen, C.; Schuele, D. Low-Frequency Dielectric Constants of α-Quartz, Sapphire, MgF_2 and MgO. *J. Appl. Phys.* **1974**, *45*, 2852−2854.

DOI: 10.1021/acs.chemmater.7b05078
Chem. Mater. 2018, 30, 7456−7463